ACS APPLIED MATERIALS & INTERFACES

December 2, 2015
Volume 7
Number 47
pubs.acs.org/acsami

Surface/interface effects on Li-ion batteries

Electrochemical preparation of textured perovskite for photovoltaics

Theory, simulation and measurement of Al_2O_3/SiGe interfaces

ACS Publications
Most Trusted. Most Cited. Most Read.

www.acs.org

ACS APPLIED MATERIALS & INTERFACES

Letter

www.acsami.org

Surface/Interface Effects on High-Performance Thin-Film All-Solid-State Li-Ion Batteries

Chen Gong,[†,‡] Dmitry Ruzmetov,[§,▽] Alexander Pearse,[‡] Dakang Ma,[‡,∥] Jeremy N. Munday,[‡,∥] Gary Rubloff,[‡,⊥] A. Alec Talin,[*,#] and Marina S. Leite[*,†,‡]

[†]Department of Materials Science and Engineering, [‡]Institute for Research in Electronics and Applied Physics, [∥]Department of Electrical and Computer Engineering, and [⊥]Institute for Systems Research, University of Maryland, College Park, Maryland 20742, United States

[§]Sensors and Electron Devices Directorate, US Army Research Laboratory, Adelphi, Maryland 20783, United States

[▽]Material Measurement Laboratory, National Institute of Standards and Technology, Gaithersburg, Maryland 20899, United States

[#]Sandia National Laboratories, Livermore, California 94550, United States

Supporting Information

ABSTRACT: The further development of all-solid-state batteries is still limited by the understanding/engineering of the interfaces formed upon cycling. Here, we correlate the morphological, chemical, and electrical changes of the surface of thin-film devices with Al negative electrodes. The stable Al−Li−O alloy formed at the stress-free surface of the electrode causes rapid capacity fade, from 48.0 to 41.5 μAh/cm^2 in two cycles. Surprisingly, the addition of a Cu capping layer is insufficient to prevent the device degradation. Nevertheless, Si electrodes present extremely stable cycling, maintaining >92% of its capacity after 100 cycles, with average Coulombic efficiency of 98%.

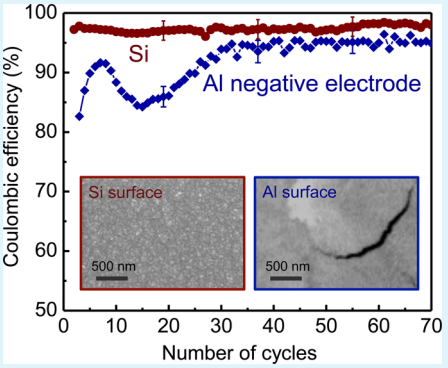

KEYWORDS: *energy storage, all-solid-state batteries, thin-films, aluminum, silicon*

In today's society, rechargeable battery technologies with improved performance are urgently needed to address the growing power and energy demands of electric and hybrid vehicles and mobile devices.[1,2] A promising alternative to conventional liquid electrolyte cells is the all-solid-state Li-ion battery (SSLIB), which provides: (i) high power density (>250 W/kg), (ii) long cycle life, (iii) inherent safety due to the absence of an organic liquid electrolyte that can cause leakage and fire, (iv) light weight and possibly compact packaging, and (v) a variety of materials that can be implemented as the electrodes including those with higher operating voltages.[3−5] As in liquid electrolyte LIBs, in all-solid-state batteries the processes at the negative electrode (commonly denoted as the anode) during the charging step can be classified into essentially 3 different types of reaction: intercalation, conversion, or alloying.[5−7] Alloying reactions usually take place between Li and certain metals or semiconductors used as negative electrodes, as $M + xLi^+ + xe^- \rightleftarrows Li_xM$, where M refers to Si, Ge, Sn, Al, and their alloys. These reactions are accompanied by substantial volume changes, which can lead to pulverization and the electrical isolation of the active layer, limiting the lifetime of the device under repeated charge/discharge cycles. Therefore, although these materials represent an attractive class of negative electrodes because of their high theoretical capacity, provided that the large strains that accompany Li alloying can be accommodated,[6] it is crucial to engineer the interfaces between the active layers of the devices to prevent undesirable irreversible reactions.

Extensive work has been realized quantifying the volume expansion/contraction during charging/discharging (lithiation/delithiation) of electrode materials in nanoscale devices,[8−10] as well as determining the morphological changes that occur during charging due to stress/strain accumulation resulting from Li alloying.[11−15] In particular, in situ transmission electron microscopy (TEM) experiments have been implemented to probe atomic scale processes in real time that take place during the battery charging and discharging.[13,16,17] Further, structural[9] and chemical characterization[17] tools have been combined to demonstrate scenarios where lithiation is irreversible. However, there is still a pressing need to identify how the negative electrode chemical composition changes upon lithiation, because it is closely related to the reversibility of the electrochemical reactions.

Aluminum, low-cost, nontoxic, and earth abundant, is a promising alternative for ultralightweight negative electrodes

Received: August 1, 2015
Accepted: October 5, 2015
Published: October 5, 2015

DOI: 10.1021/acsami.5b07058
ACS Appl. Mater. Interfaces 2015, 7, 26007−26011

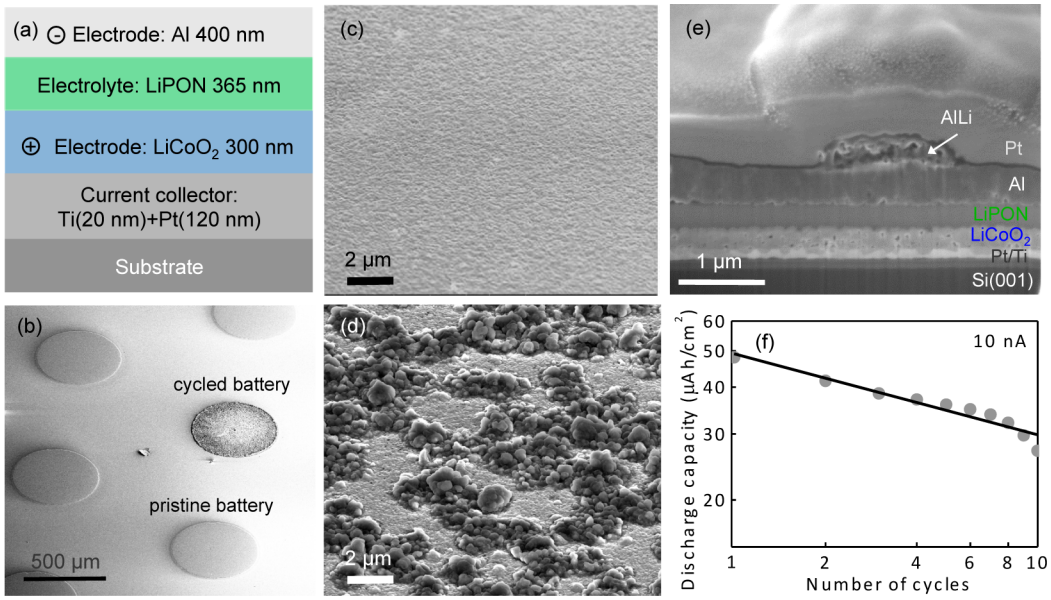

Figure 1. Al negative electrode for all-solid-state batteries. (a) Schematic of all-solid-state batteries with Al negative electrodes. (b) SEM of micron-scale devices showing morphology changes upon cycling. SEM of Al surface for (c) pristine and (d) cycled devices shown in (b). (e) Cross-section SEM image of Al electrode after 10 charging cycles, tilt = 45°. The Pt layer is added uniquely to protect the surface of the battery during the ion milling process and is not an active layer of the device. (f) Discharge capacity as a function of the number of cycles for 10 nA.

for portable devices, with theoretical capacity equal to 993 mAh/g for lithium storage.[18,19] Al metal electrodes have recently presented extremely high-rate capability (charging time of 1 min, with current density of ∼4000 mA/g), with specific capacity of about 70 mAh/g, resulting from the intercalation/deintercalation of chloroaluminate anions from the liquid electrolyte into the cathode.[20] Nevertheless, in all-solid-state devices, the alloying reaction between Al and Li leads to the formation of a very stable AlLi alloy ($Al + Li^+ + e^- \rightleftarrows AlLi$), with consequent pulverization of the negative electrode and rapid loss in capacity in nanoscale devices.[18,21] However, many details of the degradation mechanism, particularly in thin-film micrometer-size batteries remain unclear, including the effects of an intrinsic Al_2O_3 layer that covers the negative electrode surface. This oxide layer is present even when fabricating/testing the battery under high-vacuum conditions (10 Å of Al_2O_3 forms in <15 min at 1×10^{-4} Torr).[22]

In this paper, we combine X-ray photoelectron spectroscopy (XPS) with local electrical conductivity measurements to characterize the processes that occur on the Al negative electrode outer surface during lithiation in thin-film batteries with the aim of gaining deeper understanding for the rapid loss in capacity. We hypothesize that a few-monolayer thick Al−Li−O compound forms on top of the Al electrode, substantially increasing the electrical resistance at its surface, thus hindering surface-bound charge transport processes and degrading the battery's overall performance. We also demonstrate that coating the Al electrode with a Cu film without breaking vacuum does not resolve the rapid capacity loss. Finally we show that similar SSLIBs fabricated with thin-film Si negative electrodes capped with Cu exhibit remarkably stable performance, retaining >92% of their discharge capacity after 100 cycles, with an average Coulombic efficiency equal to 98%.

Thin-film SSLIBs were fabricated by sputtering 300 nm of $LiCoO_2$ as the positive electrode (140 mAh/g), 365 nm of LiPON for the electrolyte (3×10^{-6} S/cm), and 400 nm of Al (993 mAh/g) as the negative electrode and the current collector, as shown in Figure 1(a) (see Methods for detailed description of batteries' fabrication). Figures 1b−d show scanning electron microscopy (SEM) images of the morphology of the Al negative electrode surface before (pristine sample) and after cycling the battery under ultrahigh vacuum (8.5×10^{-11} Torr). The as-deposited Al surface is smooth, with roughness <20 nm. The lithiation of the Al layer, accompanied by the volume expansion of the negative electrode, results in the formation of ∼1 μm diameter mounds distributed on its surface and composed principally of AlLi alloy, as previously determined, see Figure 1e for a cross-section SEM image of all the active layers of the device (with a protective Pt capping layer deposited during the FIB process).[12] AlLi does not form in the bulk of the Al electrode, nor at the LiPON/Al interface; its formation is confined to the outer surface where the large (∼100%) volumetric strain can be best accommodated. The surface segregation of AlLi, however, does not in itself explain the rapid loss in capacity, as shown in Figure 1f.

Previously, we postulated that formation of the AlLi mounds occurred mainly by surface or grain boundary mediated diffusion, because bulk diffusion coefficients for both Li and Al are very low. Further, we suggested that loss of electrical contact with the negative electrode outer surface segregated AlLi phase did not substantially contribute to the capacity loss, because the mounds remained physically attached to the bulk Al. Because the chemical transformations that accompany charge transfer in SSLIBs with Al negative electrodes occur predominantly on the top surface and because surface diffusion paths for Al and Li are needed for cycling the battery, we have reasoned that loss of surface conductivity could degrade the battery performance. To test this hypothesis, we use conductive atomic force microscopy (c-AFM) to measure the effects of electrochemical cycling on the surface electrical conductivity of the negative electrode, as shown in Figure 2. Prior to lithiation the Al layer is highly conductive. Although the Al outer surface is covered with an intrinsic Al_2O_3 layer (Figure 2(a-b)), the oxide is sufficiently thin (∼3 nm) to allow electron tunneling

DOI: 10.1021/acsami.5b07058
ACS Appl. Mater. Interfaces 2015, 7, 26007−26011

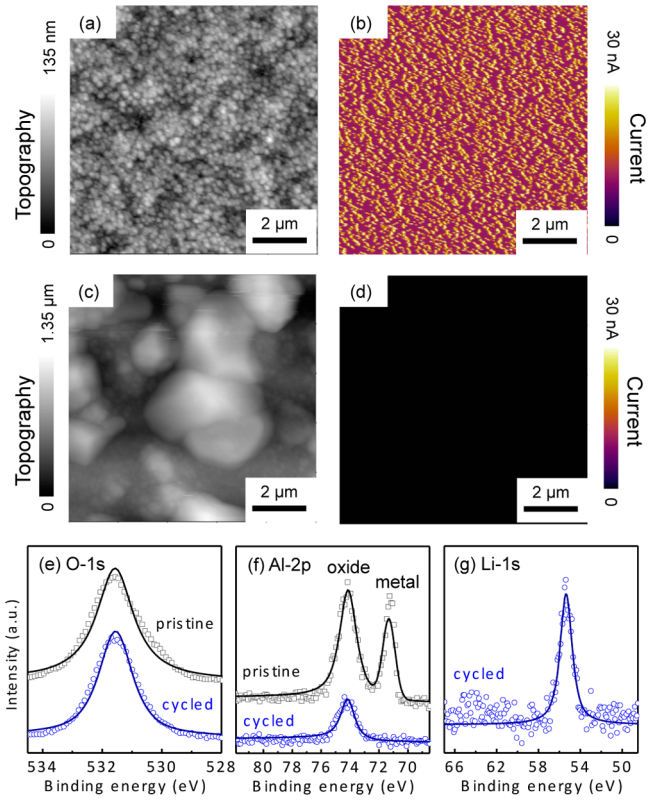

Figure 2. Al-based batteries surface characterization. Topography and conductive atomic force microscopy scans for (a, b) pristine and (c, d) cycled Al-based batteries, respectively, showing complete loss in electronic conductivity upon cycling. XPS of Al negative electrode for pristine and cycled batteries showing (e) oxygen peaks, (f) Al metal and oxide peaks, and (g) Li peak for the cycled device.

during the c-AFM measurements. Following 10 charge/discharge cycles at 30 nA, the electrode surface becomes insulating throughout and irrespective of morphology, indicating the formation of a thicker, uniformly distributed insulating layer (Figure 2c, d). The possible presence of an insulating layer on top of the Al and AlLi layers can substantially hinder the charging and discharging processes because these must be accompanied by electron flow in and out of the negative electrode, respectively.

To help identify the chemical composition of the insulating top layer, we use XPS. The O-1s signature peak at 531 eV from Al_2O_3 is present in both pristine and cycled samples (Figure 2e). The spectrum collected on a pristine battery contains both Al-2p metal and oxide peaks. However, after cycling the device 10 times, only the oxide peak is present (even at the discharge state), as shown in Figure 2f. This result indicates that upon the mounds' formation, the top layers of the electrode are no longer metallic, because of a reaction between Li and both metallic and oxidized Al as well as additional oxygen from the environment. Simultaneously, we detected the Li-1s peak at 55.3 eV, confirming that Li is present on the top surface of the Al layer even after the device is fully discharged (see Figure 2g). The XPS measurements confirm that a new material, composed by Li, Al, and O is present at the top surface of the negative electrode. Further, during the lithiation process the metallic Al from the top layers reacts with Li, suggesting that the Al−Li−O layer is at least 10 nm thick, preventing the observation of metallic Al by XPS. This insulating film impedes electronic current flow between the electrode and the probe on the c-AFM measurements. These changes in composition and electrical properties of the negative electrode surface are in agreement with a model we previously proposed, where the Li atoms react with the intrinsic Al_2O_3 layer forming a ternary alloy, as a consequence of the high diffusivity of Li in Al.[12] While the mounds are composed of porous AlLi,[12] the outer shell is formed by an insulating Al−Li−O layer.

The c-AFM and XPS measurements both suggest that cycling of the SSLIBs with Al negative electrodes leads to formation of an insulating surface oxide, which could contribute to capacity loss by preventing electron flow to the surface layers where AlLi alloy is formed. Given that additional oxygen (i.e., oxygen not present as native Al_2O_3 prior to cycling) must come from the surrounding environment, we can hypothesize that an electrically conducting film which does easily oxidize on top of the Al surface would increase the battery cycle life by preventing, or at least slowing the rate of Al−Li−O growth. To test this idea, we evaporated a 400 nm thick Cu capping layer immediately after the Al deposition without exposing the samples to the ambient. As shown in Figure 3, the Cu overlayer does not increase the

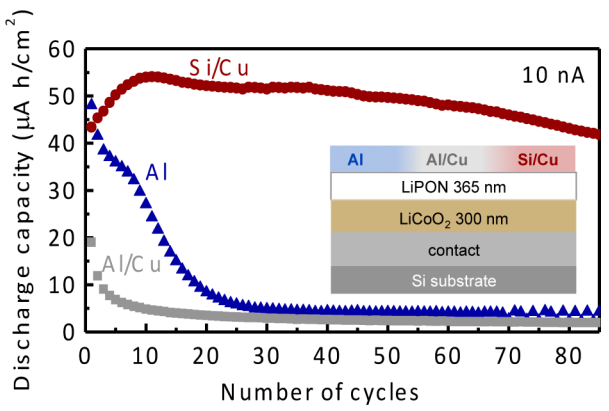

Figure 3. Electrochemical performance of thin-film all-solid-state batteries. Discharge capacity for 400 nm Al, 400 nm Al/400 nm Cu, and 50 nm Si/400 nm Cu negative electrodes, for batteries charged at 10 nA in ultrahigh vacuum, under identical conditions. Inset: schematic of solid-state devices (out of scale for clarity).

cycle life of the batteries. This result is not entirely surprising given that diffusivity of O in Cu at room temperature is $\sim 1 \times 10^{-12}$ cm^2/s,[23] which implies that it would take ~1600 s for oxygen to diffuse through the 400 nm thick Cu layer. This new result suggests that capacity fade is likely due to a combination of reasons, which include loss of surface diffusion paths for the Li in the porous AlLi alloy once the surface is oxidized, as well as loss in electrical conductivity. It is interesting to note that from the charge/discharge curves (see Figure S3), the charge cycle of the Al/Cu battery does not show a local maximum at 3.8 V compared with that of the uncapped Al-based device, strongly indicating that the existence of the Cu capping layer has altered the electrochemical reactions taking place at the negative electrode and could be another reason for the capacity fade.

Our proposed mechanism implies that if bulk Li diffusion were faster so as not to depend on surface diffusion, capacity retention could be improved. To test this point, we fabricated similar batteries with 50 nm thick Si negative electrodes[24,25] covered with 400 nm thick Cu. Like Al, Si also rapidly forms an insulating surface oxide; however, Li diffusion is ~10 orders of magnitude faster in Si compared to Al[26] and therefore does not

DOI: 10.1021/acsami.5b07058
ACS Appl. Mater. Interfaces 2015, 7, 26007−26011

depend on surface diffusion mechanism. The SSLIBs with Si electrodes are tested using exactly the same procedure as used with SSLIBs with Al. As shown in Figure 4, these batteries retained over 92% of their capacity after 90 cycles.

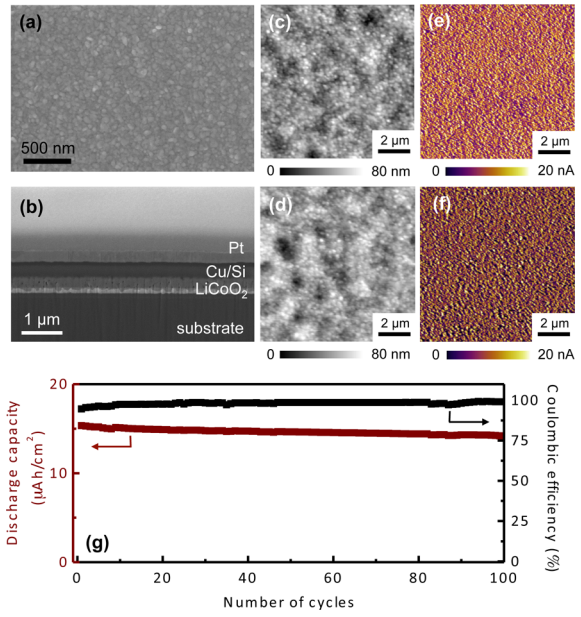

Figure 4. Electrochemical performance of thin-film all-solid-state battery with Si negative electrode. (a) Plane view and (b) cross-section SEM images of Si/Cu negative electrode after 10 charging cycles at 30 nA. A 2 μm thick Pt layer was added to prevent the damage of the Cu/Si top surface during the ion milling process for cross-sectional imaging. Topography and conductive atomic force microscopy scans for (c, e) pristine and (d, f) cycled battery, respectively, showing uniform and constant conductivity upon cycling. (g) Discharge capacity as a function of number of cycles. Capacity retention >92%, with average Coulombic efficiency = 98%.

Figure 4 shows the morphology and the electrical analysis of the Si negative electrode after cycling the battery in ultra high vacuum and its electrochemical profile. After cycling the device, the interface between the electrolyte and the Si does not present any accumulation of Li,[27] as shown in the cross-section SEM image of Figure 4b. c-AFM measurements show that the electrical properties of the Si/Cu layer are unaltered upon cycling the battery (see Figure 4c–f). The Si/Cu battery shows an excellent performance, with discharge capacity of ~15 μAh/cm^2 after 100 cycles at 30 nA (Figure 4g). As a consequence, the Coulombic efficiency of the device is near 100%. This remarkable improvement in performance is due to the fact that Li diffuses almost 10 orders of magnitude faster in Si than it does in Al,[26] and thus the formation of the surface mounds and the associated trapped Li does not occur in Si (or at a much lower level). Additionally, an insulating compound analogous to the Al–O–Li, i.e., Si–O–Li does not seem to form on the Si electrode surface (see Figure S2). The SSLIB with Si has an electrochemical performance similar to micron- and nanoscale size electrodes,[28,29] with high cycling stability despite the large volume change that takes place during lithiation. Furthermore, given the same Cu capping layer, the Si-based SSLIB still outperforms the Al/Cu system regarding the capacity retention after long-time cycling. One possible reason for the limited performance of the Al/Cu battery is that the diffusion of Cu into Al may lead to the loss of lithium diffusion path along the Al grain boundaries that constitute the negative electrode, because Cu does not react with lithium ion at low electrical potential.[30] Moreover, as mentioned before, Li diffusion is much faster in Si than in Al; therefore, the potential loss of diffusion path along the grain boundaries in the Si film may not have a significant effect on its electrochemical performance. More detailed studies as to how much each factor contributes to the battery overall performance, such as probing a SSLIB with a thick layer of Al_2O_3 and using a current collector with a substantially different coefficient of thermal expansion as the Al, is planned for the near future.

Our systematic study revealed that the Al/Al_2O_3 is the limiting interface for the Li reversible diffusion in SSLIB, instead of the electrolyte/electrode interface. Previously, a P–Si interdiffused layer has been observed at the LiPON/Si electrolyte/negative electrode interface during nanobattery overcharging.[13] However, for the micrometer-scale devices like the ones probed here, the effect of this interface is negligible compared to the total volume of the negative electrode. For the thin-film SSLIB containing Al, the surface of the material substantially changes upon cycling, forming a new material (Al–Li–O) that traps Li, according to the following chemical reaction

$$(1+x)\mathrm{Li} + \left(1-\frac{x}{3}\right)\mathrm{Al} + \left(\frac{x}{6}+\frac{y}{2}\right)\mathrm{Al_2O_3} \rightarrow \mathrm{Li}_x\mathrm{Al}_y\mathrm{O}_{(x+3y)/2} + \mathrm{AlLi}$$

This alloy substantially reduces the surface diffusion paths for the Li in the porous AlLi. Further, even after discharging the batteries, the Al–Li–O is still stuck at the surface of the electrode, indicating that this material is thermodynamically stable and that the alloying reaction with Li is not reversible.

Summarizing, we investigated the degradation of SSLIBs with Al and Si negative electrodes and identified substantial Li accumulation at the top surface of the Al electrode, accompanied by morphological and electrical changes. The Al layer showed fast capacity fade possibly caused by the formation of a ternary Al–Li–O alloy at the top surface of the negative electrode, as confirmed by XPS measurements. This ternary alloy is thermodynamically stable, does not decompose upon battery discharging, and forms an insulating barrier at the top surface of the electrode, as indicated by c-AFM measurements. The addition of a Cu protective film did not prevent the capacity loss, due to the presence of an Al_2O_3 thin layer between the negative electrode and the Cu layers, and the sufficiently rapid oxygen diffusion in Cu at room temperature. By comparison, thin-film Si electrodes showed excellent performance up to 100 cycles, retaining >92% of its discharge capacity, with stable Coulombic efficiency of 98%. The results presented here show the importance of electrode surface and current collector/electrode interface reactions in SSLIB, in addition to those occurring at the electrode/electrolyte interfaces, which are typically the focus of investigation in liquid electrolyte LIBs.

■ ASSOCIATED CONTENT

Supporting Information

The Supporting Information is available free of charge on the ACS Publications website at DOI: 10.1021/acsami.5b07058.

Experimental details of battery fabrication, XPS and c-AFM measurements, cross-section SEM of batteries,

DOI: 10.1021/acsami.5b07058
ACS Appl. Mater. Interfaces 2015, 7, 26007–26011

cycling curves and Coulombic efficiency for Al and Si negative electrode batteries (PDF)

AUTHOR INFORMATION

Corresponding Authors

*E-mail: mleite@umd.edu.

*E-mail: aatalin@sandia.gov.

Notes

The authors declare no competing financial interest.

ACKNOWLEDGMENTS

MSL and JNM thank the financial support from the School of Engineering at the University of Maryland, and the Minta Martin Award. CG acknowledge the University of Maryland 2015 Graduate School's Summer Research Fellowship program. This work was partially supported by the Laboratory Directed Research and Development Program at Sandia National Laboratories. Sandia is a multiprogram laboratory operated by Sandia Corporation, a Lockheed Martin Company, for the U.S. DOE National Nuclear Security Administration under Contract DE-AC04-94AL85000. Nanostructures for Electrical Energy Storage (NEES), an Energy Frontier Research Center funded by the U.S. Department of Energy, Office of Science, and Office of Basic Energy Sciences under award DESC0001160, provided partial support to AAT and GR for data analysis and manuscript authoring, and to AP for carrying out XPS experiments and analysis.

REFERENCES

(1) Whittingham, M. S. Lithium Batteries and Cathode Materials. *Chem. Rev.* **2004**, *104*, 4271−4302.

(2) Magasinski, A.; Dixon, P.; Hertzberg, B.; Kvit, A.; Ayala, J.; Yushin, G. High-Performance Lithium-Ion Anodes Using a Hierarchical Bottom-up Approach. *Nat. Mater.* **2010**, *9*, 353−358.

(3) Kim, T. H.; Park, J. S.; Chang, S. K.; Choi, S.; Ryu, J. H.; Song, H. K. The Current Move of Lithium Ion Batteries Towards the Next Phase. *Adv. Energy Mater.* **2012**, *2*, 860−872.

(4) Oudenhoven, J. F. M.; Baggetto, L.; Notten, P. H. L. All-Solid-State Lithium-Ion Microbatteries: A Review of Various Three-Dimensional Concepts. *Adv. Energy Mater.* **2011**, *1*, 10−33.

(5) Dudney, N. J. Solid-State Thin-Film Rechargeable Batteries. *Mater. Sci. Eng., B* **2005**, *116*, 245−249.

(6) Obrovac, M. N.; Chevrier, V. L. Alloy Negative Electrodes for Li-Ion Batteries. *Chem. Rev.* **2014**, *114*, 11444−11502.

(7) Erickson, E. M.; Ghanty, C.; Aurbach, D. New Horizons for Conventional Lithium Ion Battery Technology. *J. Phys. Chem. Lett.* **2014**, *5*, 3313−3324.

(8) Ruzmetov, D.; Oleshko, V. P.; Haney, P. M.; Lezec, H. J.; Karki, K.; Baloch, K. H.; Agrawal, A. K.; Davydov, A. V.; Krylyuk, S.; Liu, Y.; Huang, J. Y.; Tanase, M.; Cumings, J.; Talin, A. A. Electrolyte Stability Determines Scaling Limits for Solid-State 3d Li Ion Batteries. *Nano Lett.* **2012**, *12*, 505−511.

(9) Qi, Y.; Harris, S. J. In Situ Observation of Strains During Lithiation of a Graphite Electrode. *J. Electrochem. Soc.* **2010**, *157*, A741.

(10) Oleshko, V. P.; Lam, T.; Ruzmetov, D.; Haney, P.; Lezec, H. J.; Davydov, A. V.; Krylyuk, S.; Cumings, J.; Talin, A. A. Miniature All-Solid-State Heterostructure Nanowire Li-Ion Batteries as a Tool for Engineering and Structural Diagnostics of Nanoscale Electrochemical Processes. *Nanoscale* **2014**, *6*, 11756−11768.

(11) Orsini, F.; Du Pasquier, A.; Beaudoin, B.; Tarascon, J. M.; Trentin, M.; Langenhuizen, N.; De Beer, E.; Notten, P. In Situ Scanning Electron Microscopy (SEM) Observation of Interfaces within Plastic Lithium Batteries. *J. Power Sources* **1998**, *76*, 19−29.

(12) Leite, M. S.; Ruzmetov, D.; Li, Z.; Bendersky, L. A.; Bartelt, N. C.; Kolmakov, A.; Talin, A. A. Insights into Capacity Loss Mechanisms of All-Solid-State Li-Ion Batteries with Al Anodes. *J. Mater. Chem. A* **2014**, *2*, 20552−20559.

(13) Santhanagopalan, D.; Qian, D.; McGilvray, T.; Wang, Z.; Wang, F.; Camino, F.; Graetz, J.; Dudney, N.; Meng, Y. S. Interface Limited Lithium Transport in Solid-State Batteries. *J. Phys. Chem. Lett.* **2014**, *5*, 298−303.

(14) Gong, C.; Bai, Y.-J.; Feng, J.; Tang, R.; Qi, Y.-X.; Lun, N.; Fan, R.-H. Enhanced Electrochemical Performance of FeWO4 by Coating Nitrogen-Doped Carbon. *ACS Appl. Mater. Interfaces* **2013**, *5*, 4209−4215.

(15) Brazier, A.; Dupont, L.; Dantras-Laffont, L.; Kuwata, N.; Kawamura, J.; Tarascon, J. M. First Cross-Section Observation of an All Solid-State Lithium-Ion "Nanobattery" by Transmission Electron Microscopy. *Chem. Mater.* **2008**, *20*, 2352−2359.

(16) Liu, X. H.; Huang, J. Y. In Situ Tem Electrochemistry of Anode Materials in Lithium Ion Batteries. *Energy Environ. Sci.* **2011**, *4*, 3844−3860.

(17) Holtz, M. E.; Yu, Y.; Gunceler, D.; Gao, J.; Sundararaman, R.; Schwarz, K. A.; Arias, T. A.; Abruña, H. D.; Muller, D. A. Nanoscale Imaging of Lithium Ion Distribution During in Situ Operation of Battery Electrode and Electrolyte. *Nano Lett.* **2014**, *14*, 1453−1459.

(18) Hudak, N. S.; Huber, D. L. Size Effects in the Electrochemical Alloying and Cycling of Electrodeposited Aluminum with Lithium. *J. Electrochem. Soc.* **2012**, *159*, A688.

(19) Lindsay, M. J.; Wang, G. X.; Liu, H. K. Al-Based Anode Materials for Li-Ion Batteries. *J. Power Sources* **2003**, *119*, 84−87.

(20) Lin, M.-C.; Gong, M.; Lu, B.; Wu, Y.; Wang, D.-Y.; Guan, M.; Angell, M.; Chen, C.; Yang, J.; Hwang, B.-J.; Dai, H. An Ultrafast Rechargeable Aluminium-Ion Battery. *Nature* **2015**, *520*, 324−328.

(21) Liu, Y.; Hudak, N. S.; Huber, D. L.; Limmer, S. J.; Sullivan, J. P.; Huang, J. Y. In Situ Transmission Electron Microscopy Observation of Pulverization of Aluminum Nanowires and Evolution of the Thin Surface Al2O3 Layers During Lithiation−Delithiation Cycles. *Nano Lett.* **2011**, *11*, 4188−4194.

(22) Cabrera, N.; Mott, N. Theory of the Oxidation of Metals. *Rep. Prog. Phys.* **1949**, *12*, 163−184.

(23) Magnusson, H.; Frisk, K. *Self-Diffusion and Impurity Diffusion in the Hydrogen, Oxygen, Sulphur and Phosphorous in Copper*; Swedish Nuclear Waste Management Company Technical Report TR-13-24 ; Swedish Nuclear Waste Management Company: Stockholm, Sweden, 2013.

(24) Zhang, W.-J. A Review of the Electrochemical Performance of Alloy Anodes for Lithium-Ion Batteries. *J. Power Sources* **2011**, *196*, 13−24.

(25) Abel, P. R.; Lin, Y.-M.; Celio, H.; Heller, A.; Mullins, C. B. Improving the Stability of Nanostructured Silicon Thin Film Lithium-Ion Battery Anodes through Their Controlled Oxidation. *ACS Nano* **2012**, *6*, 2506−2516.

(26) Tritsaris, G. A.; Zhao, K.; Okeke, O. U.; Kaxiras, E. Diffusion of Lithium in Bulk Amorphous Silicon: A Theoretical Study. *J. Phys. Chem. C* **2012**, *116*, 22212−22216.

(27) Korgel, B. A. Nanomaterials Developments for Higher-Performance Lithium Ion Batteries. *J. Phys. Chem. Lett.* **2014**, *5*, 749−750.

(28) Song, J.; Zhou, M.; Yi, R.; Xu, T.; Gordin, M. L.; Tang, D.; Yu, Z.; Regula, M.; Wang, D. Interpenetrated Gel Polymer Binder for High-Performance Silicon Anodes in Lithium-Ion Batteries. *Adv. Funct. Mater.* **2014**, *24*, 5904−5910.

(29) Yi, R.; Dai, F.; Gordin, M. L.; Sohn, H.; Wang, D. Influence of Silicon Nanoscale Building Blocks Size and Carbon Coating on the Performance of Micro-Sized Si−C Composite Li-Ion Anodes. *Adv. Energy Mater.* **2013**, *3*, 1507−1515.

(30) Wakihara, M. Recent Developments in Lithium Ion Batteries. *Mater. Sci. Eng., R* **2001**, *33*, 109−134.

DOI: 10.1021/acsami.5b07058
ACS Appl. Mater. Interfaces 2015, 7, 26007−26011

Supporting Information

Surface/Interface Effects on High-Performance Thin-Film All-Solid-State Li-Ion Batteries

Chen Gong[1,2], Dmitry Ruzmetov[3], Alexander Pearse[2], Dakang Ma[2,4], Jeremy N. Munday[2,4], Gary Rubloff[2,5], A. Alec Talin[6], Marina S. Leite[1,2*]*

[1]Department of Materials Science and Engineering, Univ. of Maryland, College Park, MD, United States.
[2]Institute for Research in Electronics and Applied Physics, Univ. of Maryland, College Park, MD, United States.
[3]Army Research Laboratory, MD, United States.
[4]Department of Electrical and Computer Engineering, Univ. of Maryland, College Park, MD, United States.
[5]Institute for Systems Research, Univ. of Maryland, MD, United States.
[6]Sandia National Laboratories, Livermore, CA, United States.

* To whom correspondence should be addressed: mleite@umd.edu, aatalin@sandia.gov

Experimental Methods

All-solid-state battery fabrication. The samples were fabricated on a Si (001) substrate with a 100 nm thick SiO_2 layer. 20 nm of Ti and 120 nm of Pt were used as the bottom contact for current collection. 300 nm of crystalline $LiCoO_2$ (cathode) was deposited by sputtering in the same chamber and without exposure to air. The sample was then annealed in ambient oxygen at 700 ^oC for 2 hours to smooth the cathode layer. Following the heat treatment, the sample was sputter coated with 365 nm of LiPON (electrolyte) and finally Al, Al/Cu, and Si/Cu negative electrode. Batteries with 0.51 mm in diameter were fabricated by using a steel mask for the top electrode deposition. All solid-state Li-ion batteries were cycled under ultra-high vacuum, at 8.5×10^{-11} Torr, to prevent any undesired chemical reactions of lithium on the top surface of the negative electrode, and to exclude the possible influence of humidity on the device degradation.

High-resolution XPS measurements. The XPS data were collected using a 12 kV monochromated Al Kα X-ray source (1486.6 eV), and the analyzer was in hybrid lens mode for survey spectra. High-resolution spectra were collected in the same mode using a step size of 0.1 eV and pass energy of 20 eV. For all measurements, the analysis spot size was 220 μm in diameter as defined by the instrument electron optics. The charge neutralization system was used and all spectra were calibrated to the C 1s hydrocarbon peak at 284.8 eV.

Conductive AFM measurements. The c-AFM measurements were carried out at room temperature using a diamond-coated probe with 83 ± 17 nm in diameter and a cantilever with force constant of 2.8 N/m, at ambient environment. During the measurements, the c-AFM probe was in contact with the negative electrode top surface and the current collector located underneath the positive electrode was grounded. The current pathway was then across all the active layers of the thin-film solid-state-battery. Scans were acquired by using a piezo scanner in closed loop, at 0.4 sec/line. The topography and current signals were acquired simultaneously, in contact mode, under 10 V bias applied to the probe.

X-section SEM imaging of batteries. 2 μm thick film of electron-beam and ion-beam Pt was initially deposited to protect the negative electrode surface during the milling process for cross-sectional imaging. Then, the samples were milled by Ga focused ion beam (FIB), using low current to minimize sample damage (9.3 and 0.8 nA).

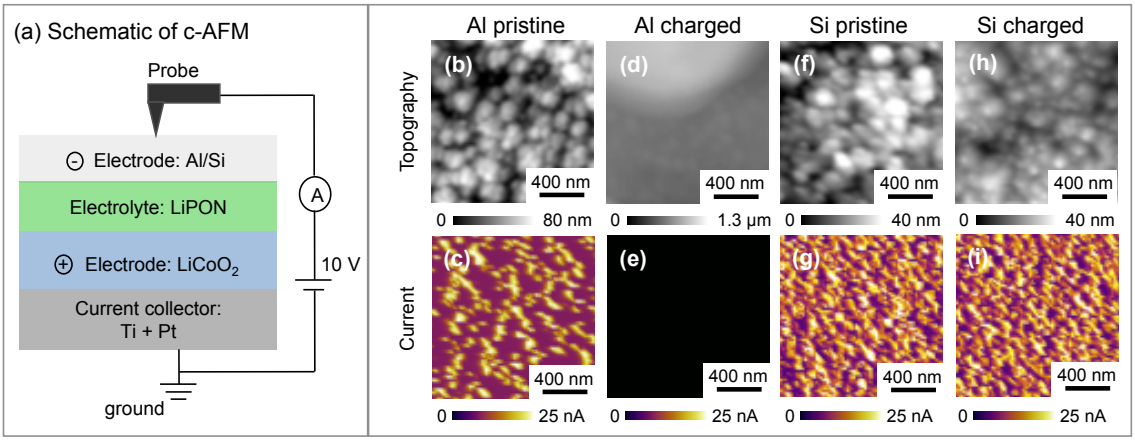

Figure S1. Conductive atomic force microscopy (c-AFM): (a) Illustration of c-AFM measurements performed on thin-film all-solid-state batteries. The measurements were carried out at room temperature using a diamond-coated probe with 83±17 nm in diameter and a cantilever with force constant of 2.8 N/m, at ambient environment. During the measurements, the c-AFM probe was in contact with the negative electrode top surface, and the current collector located underneath the positive electrode was grounded. The current pathway was then across all the active layers of the thin-film solid-state-battery. Scans were acquired by using a piezo scanner in closed loop. The topography and current signals were acquired simultaneously, in contact mode, while 10 V was applied to the probe. (b-i) Topography and current maps for thin-film batteries with Al and Si negative electrodes.

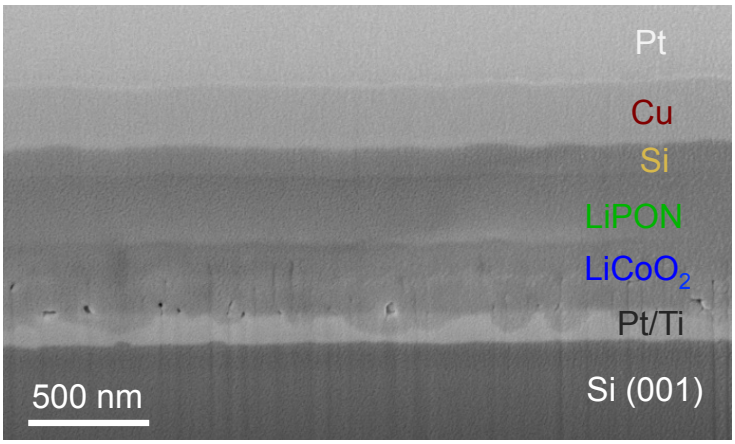

Figure S2. Si-based thin-film batteries. Cross-section SEM image of Si-based thin-film all-solid-state battery after 10 cycles at 30 nA, showing smooth interface between the active layers of the device. The Pt layer was added uniquely to protect the surface of the battery during the ion milling process and is not an active layer of the device. SEM settings: 5 kV, 0.10 nA, detector: secondary electron (SE), image tilt = 52°.

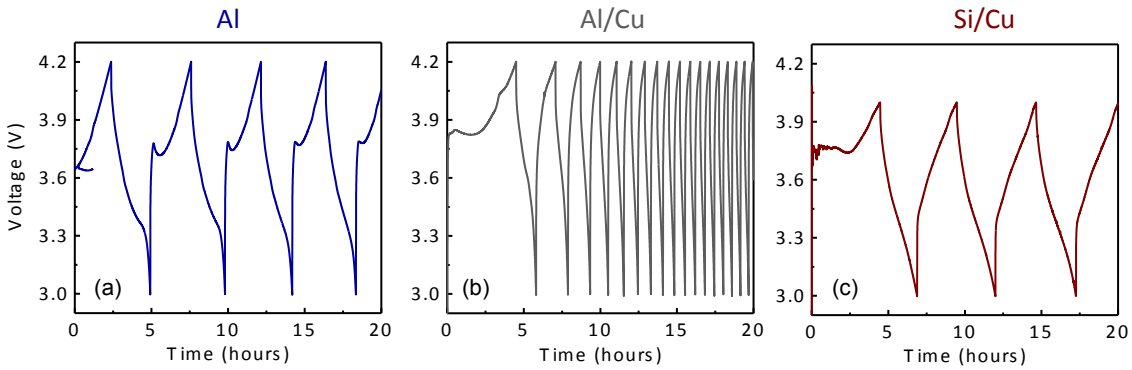

Figure S3. Cycling curves for thin-film solid-state batteries with (a) Al, (b) Al/Cu, and (c) Si/Cu negative electrodes, charged at 10 nA.

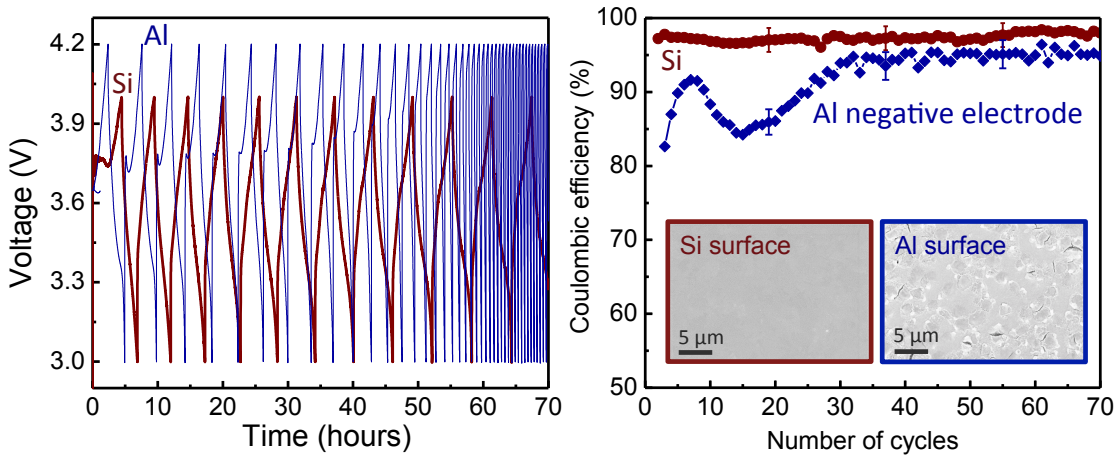

Figure S4. (Left) Voltage profile of Al (blue) and Si (red) negative electrode batteries showing the fast degradation of the Al-based device and the high-stability of the Si-based one. (Right) Coulombic efficiency for the same devices. Inset shows SEM images of the outer surface of the two electrodes.